

Automatic selection of the best neural architecture for time series forecasting via multi-objective optimization and Pareto optimality conditions

Qianying Cao^a, Shanqing Liu^a, Alan John Varghese^b, Jerome Darbon^a, Michael Triantafyllou^c,
George Em Karniadakis^{a,*}

^a*Division of Applied Mathematics, Brown University, Providence, RI 02906, U.S.A.*

^b*School of Engineering, Brown University, Providence, RI 02906, U.S.A.*

^c*Department of Mechanical Engineering, Massachusetts Institute of Technology, Cambridge, MA 02139, U.S.A.*

Abstract

Time series forecasting plays a pivotal role in a wide range of applications, including weather prediction, healthcare, structural health monitoring, predictive maintenance, energy systems, and financial markets. While models such as LSTM, GRU, Transformers, and State-Space Models (SSMs) have become standard tools in this domain, selecting the optimal architecture remains a challenge. Performance comparisons often depend on evaluation metrics and the datasets under analysis, making the choice of a universally optimal model controversial. In this work, we introduce a flexible automated framework for time series forecasting that systematically designs and evaluates diverse network architectures by integrating LSTM, GRU, multi-head Attention, and SSM blocks. Using a multi-objective optimization approach, our framework determines the number, sequence, and combination of blocks to align with specific requirements and evaluation objectives. From the resulting Pareto-optimal architectures, the best model for a given context is selected via a user-defined preference function. We validate our framework across four distinct real-world applications. Results show that a single-layer GRU or LSTM is usually optimal when minimizing training time alone. However, when maximizing accuracy or balancing multiple objectives, the best architectures are often composite designs incorporating multiple block types in specific configurations. By employing

*Corresponding author.

Email addresses: qianying_cao@brown.edu (Qianying Cao), shanqing_liu@brown.edu (Shanqing Liu), alan_john_varghese@brown.edu (Alan John Varghese), jerome_darbon@brown.edu (Jerome Darbon), mistetri@mit.edu (Michael Triantafyllou), george_karniadakis@brown.edu (George Em Karniadakis)

a weighted preference function, users can resolve trade-offs between objectives, revealing novel, context-specific optimal architectures. Our findings underscore that no single neural architecture is universally optimal for time series forecasting. Instead, the best-performing model emerges as a data-driven composite architecture tailored to user-defined criteria and evaluation objectives.

Keywords: recurrent neural networks, transformers, states-space models, Pareto optimality

1. Introduction

Time series forecasting plays an important role across diverse fields, including weather prediction, structural health monitoring, financial markets, among others. For example, real-time forecasting of ocean currents and waves helps to ensure operational safety in offshore oil drilling. Accurate real-time forecasting of electricity demand may help to prevent possible regional blackouts. Hence, developing an efficient model that can forecast time series reliably is crucial health monitoring systems and a basic capability of digital twins of engineering systems but also in other domains, e.g., weather and environment, healthcare, finance and economics, etc.

There are a multitude of existing models to forecast time series [1–8], designed primarily around the autoregressive model (AR) or the autoregressive integrated moving average model (ARIMA) [1]. These models learn the correlation between history data and future data, and use it in various forms for predicting future values. However, traditional models assume linear relationships between historical observations and future values, which limits their ability to handle nonlinear dynamics commonly present in real engineering problems. To overcome the limitations of traditional methods, many deep learning approaches have been developed [9–13], which show significant advantages in modeling complex and non-linear systems. Long short-term memory (LSTM) [14] was proposed in 1997 to mitigate the vanishing gradient problem in traditional recurrent neural networks, and advanced versions [15–17] were developed to solve different engineering problems [18–22]. Compared with LSTM, Gated recurrent unit (GRU) [23], which has a gating mechanism to input but lacks an output gate, employs fewer parameters. Chung et al. [24] evaluated RNN, LSTM and GRU on polyphonic music modeling and speech signal modeling, which revealed GRU was comparable to LSTM. Systematic studies of these recurrent networks applied to dynamical systems were performed in [25–27].

The Transformer architecture, which is based solely on Attention mechanisms, is very popular in translation tasks since it was first proposed in 2017 [28]. The multi-headed self-Attention replaces the recurrent layers which are typically used in encoder-decoder architectures. Based on the self-Attention mechanisms in Transformer, Wu et al. [29] proposed a novel method to learn complex dynamics of various lengths from time series data. Subsequently, a series of applications of Transformers in different domains were developed [30–37]. For example, Pokhrel et al. [38] presented a Transformer-based regression scheme to forecast significant wave heights in oceans, demonstrating that their proposed method outperforms previous machine learning methods, such as CNN and LSTM. However, Zeng et al. [39] questioned the effectiveness of the Transformer architecture in time series forecasting. To avoid the Transformer’s computational inefficiency on long sequences, Gu and Dao [40] proposed Mamba, which integrated selective state-space models (SSMs) into a simple network architecture without Attention, achieving fast inference and better performance than the Transformer models on diverse application domains. Some advanced type of Mamba and their applications were quickly developed [41–43]. Wang et al. [44] presented Simple-Mamba for time series forecasting, proving that in thirteen experiments Simple-Mamba reduced the computational cost and obtained better performance. To explore the application of SSMs in time series forecasting, Hu et al. [45] proposed Time-SSM which had much fewer parameters than Mamba. Hu et al. [46] demonstrated the superior performance of Mamba compared to other models in terms of both lowest computational cost and excellent extrapolation capabilities for operator learning of dynamical systems. The superior performance of Mamba compared to standard Transformers was also demonstrated by Cheng et al. [47].

From the literature, it is evident that LSTM, GRU, Transformer and Mamba are the most widely used neural network models for time series forecasting, and each of them exhibits unique characteristics. However, determining the “best” model remains challenging, since performance comparisons often vary depending on the evaluation metrics and datasets employed. Moreover, hybrid models which combine these architectures have emerged [48–53], which significantly expand the design space of network architectures and complicate the task of selecting the optimal model for specific applications. These available models can overwhelm researchers and engineers, making it difficult

to assess their relative performance and select the right model.

In this paper, we establish an automated general framework that seeks to find the best composite architectures, incorporating LSTM blocks, GRU blocks, multi-Attention blocks and SSM blocks. The number of each type of blocks and the sequence of these blocks are regarded as hyperparameters. This flexible framework not only includes many existing models but most importantly it designs automatically new network models that do not exist in the literature. Additionally, each architecture requires tuning other hyperparameters, such as the hidden dimension. This naturally raises the question of how to select the optimal architecture. To address this challenge, we propose a multi-objective optimization (MOO) method to automatically design the best network architecture with the best hyperparameters. In particular, we first parameterize the construction of different architectures within a specific domain. Subsequently, we model the performance of these architectures using a vector-valued map, which maps a parameterized architecture to objectives that reflect its performance, such as relative \mathcal{L}_2 error, training time, and the number of parameters. The selection of best architecture is then formulated as a multi-objective optimization problem, in the sense of minimizing this vector-valued map. We first identify the set of Pareto optimal architectures, and subsequently, based on a user-defined preference function, we discover the best architecture. We also propose a Linear Programming (LP) approach to rediscover a particular architecture among the ones on the Pareto front.

The remainder of the paper is organized as follows: In [section 2](#), we introduce the architecture of the composite model. In [section 3](#) we present the MOO and Pareto-optimality based method, and the preference function approach for the selection of best architecture. In [section 4](#) to [section 7](#), we apply our model to four real-world applications, and we discuss the key findings. Finally, in [section 8](#) we summarize the present work and provide concluding remarks.

2. Composite Architectures

We propose to search for composite architectures, which are hybrids consisting of GRU, LSTM, multi-head Attention and SSM blocks to leverage the best features of each while pursuing the objectives that a specific engineering or another application needs. The number and the sequence of

each type of block are tunable parameters, which will be obtained based on multi-objective optimization method, aiming to design the best architectures tailored to specific engineering needs and target objectives.

The model architecture is shown in [Figure 1](#), which includes three main modules. Two linear transformations can be used in the first (Embedding) and the third (LN) modules, which lift the input to a higher dimensional representation and project the output to the original dimension, respectively. The second module is the main step, which hybridizes GRU, LSTM, multi-head Attention and SSM blocks. Note that [Figure 1](#) only demonstrates one possible scenario about the number and sequence of each block. A plurality of architectures can be created based on this composite model. Each LSTM block includes a hidden state and a cell state, which are updated during each time step. The GRU block is similar to the LSTM block but includes fewer gates so that fewer parameters are used. The readers are referred to Refs. [14, 23] for the details of these architectures. [Figure 1\(b\)](#) and (c) demonstrate the architectures of a Transformer block and a SSM block, which consist of two sequential residual modules. In the first module, the input undergoes layer normalization first. Then, we apply a multi-head Attention or SSM mechanism to enable the model to focus on the input sequence in parallel. The resulting output is then added to the original input by a residual connection. Similarly, the output of the first module passes a layer norm and a feed-forward neural network (FFN) in the second module, whose output is added to the module's input by another residual connection. Note that both the Transformer and SSM blocks use the Pre-LN model, which puts the layer normalization inside the residual blocks and converges much faster than the traditional method [54].

To design the optimal architecture based on the composite model and the multi-objective optimization method, the parameterized spaces of different architectures are considered. The number of each block is defined as a vector $\mathbf{x}_1 = [n, m, j, k]$, where n, m, j and k represent the number of GRU, LSTM, multi-head Attention and SSM blocks, respectively. The sequence of blocks is represented by x_2 , which is chosen from a discrete set of integers $[1, 2, \dots, p - 1, p]$. Each integer represents a specific sequence. For example, the sequence of blocks is [SSM, Attention, GRU, LSTM] when $x_2 = 1$ and it is [Attention, SSM, GRU, LSTM] when $x_2 = 2$. The integer p represents the total number of sequences, which will be determined based on the specific problem we solve. By combin-

ing GRU, LSTM, multi-head Attention and SSM blocks, and considering the number and sequence of blocks as tunable parameters, the proposed model not only includes many existing architectures but also can discover a wide range of new and optimal architectures.

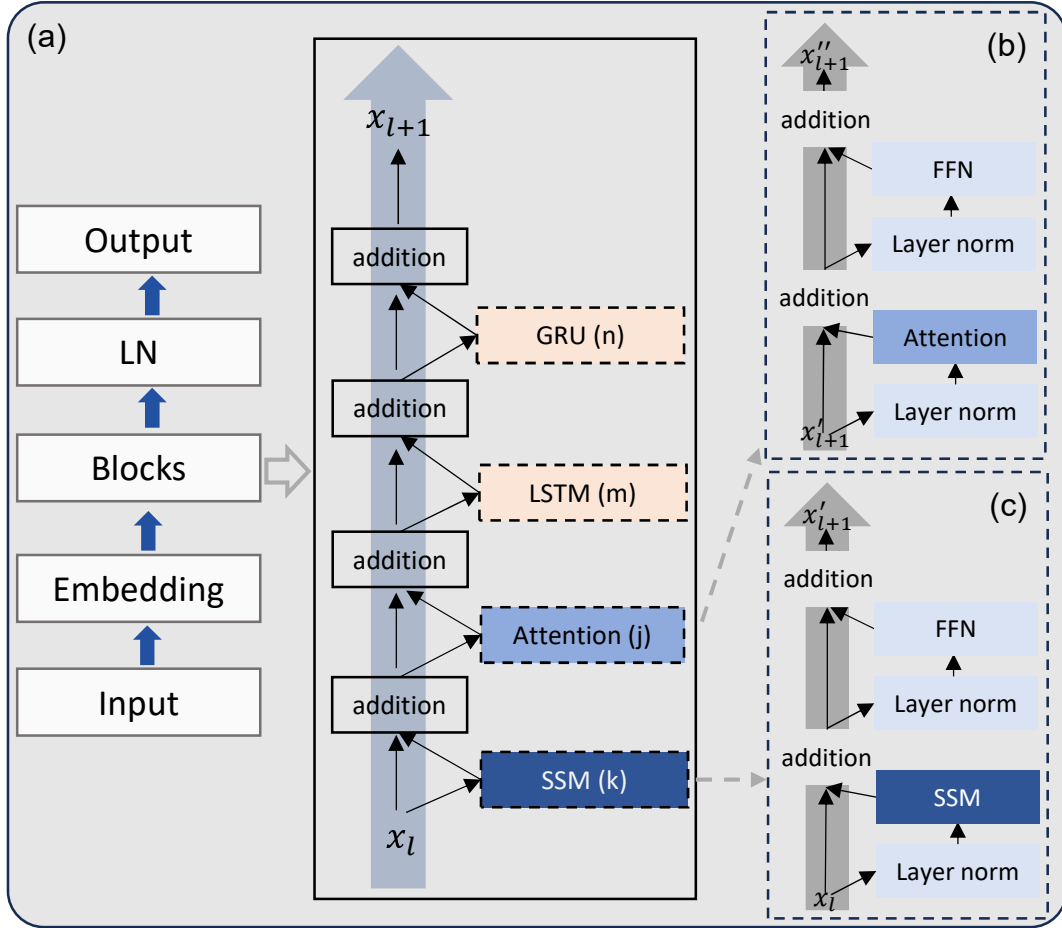


Figure 1: A schematic representation of the entire architecture (a) of the composite model with details on the type of blocks, e.g., the attention mechanism in (b) and the SSM module in (c).

3. Multi-Objective Optimization and Selection of Architectures

In this section, we define the performance map for parameterized architectures. The selection of the best architecture is formulated as a multi-objective optimization problem. A family of architectures are then selected in the Pareto optimal sense. We also present the discovery and rediscovery of a particular optimal architecture by the preference function.

3.1. Multi-objective optimization and Pareto optimality

Consider, in general, a multi-objective optimization problem to minimize a vector valued map $J : X \rightarrow \mathbb{R}^N$:

$$\min_{x \in X} J(x) := [J_1(x), J_2(x), \dots, J_N(x)]^T. \quad (1)$$

In general, problem (1) does not necessarily admit a solution x^* that minimizes all the objective functionals $\{J_i\}_{i \in \{1, 2, \dots, N\}}$. A standard concept of solution for MOO problems is known as Pareto optimal solution. The definitions of Pareto optimal solution and Pareto front are as follows.

- Definition 1.**
1. For every $x^1, x^2 \in X$, we say that x^1 dominates x^2 if and only if $J_i(x^1) \leq J_i(x^2)$, for every $i \in \{1, 2, \dots, N\}$, and there exists at least one k such that $J_k(x^1) < J_k(x^2)$.
 2. We say that $x \in X$ is a Pareto optimal solution if and only if there is no other element in X that dominates x . We denote by $\mathcal{P}_J(X)$ the set of Pareto optimal solutions.
 3. We call the Pareto front $\mathcal{F}_J(X)$ the image of the set of Pareto optimal solutions $\mathcal{P}_J(X)$ by the objective function f , that is, $\mathcal{F}_J(X) = \{J(x) \mid x \in \mathcal{P}_J(X)\}$.

Note that the Pareto optimal and Pareto front can also be defined in the weak sense (see for instance [55]), where strict inequalities are considered in Definition 1.

3.2. Selection of Best Architecture

Let us denote by \mathcal{S} the parameterized space of different architectures. Note that \mathcal{S} may vary depending on the context and tasks. We will provide a detailed description of this parameterized domain \mathcal{S} in [section 4](#) – [section 7](#) for specific examples.

We evaluate the performance of different architectures based on three criteria: (1) relative \mathcal{L}_2 error computed after applying the architecture to solve the real problem; (2) training time; and (3) number of parameters. These criteria can be modeled and quantified by a vector-valued performance map $f : \mathcal{S} \rightarrow \mathbb{R}^3$, where given an architecture $x \in \mathcal{S}$, $f_1(x)$ denotes the relative \mathcal{L}_2 error, $f_2(x)$ denotes the training time, and $f_3(x)$ is the number of parameters.

As typically one wants to minimize all the aforementioned performance criteria, the selection of best architecture can then be formulated by a MOO problem such that:

$$\min_{x \in \mathcal{S}} f(x) := [f_1(x), f_2(x), f_3(x)]^T. \quad (2)$$

We intend to identify the Pareto optimal architectures in the sense of optimization problem (2). Note that the MOO and Pareto optimal framework can be easily adapted when one wants to extend the domain \mathcal{S} , i.e., including more architectures, or extend the dimension of image set, i.e., considering more performance criteria.

3.3. Discovery of Optimal Architectures

We consider a preference function based discovery approach for finding the best architecture among the Pareto candidates.

Definition 2. *For a particular user, the discovery of optimal architecture refers to finding the best designed architecture that fits his preference.*

In particular, the user's preference on the criteria is modeled by a preference function, $p : \mathbb{R}^3 \rightarrow \mathbb{R}$, that maps the image set performance map f to \mathbb{R} . Using this preference function, the selection of the best architecture among Pareto optimal ones is reduced to a classical optimization problem of the form:

$$\min_{x \in \mathcal{P}_f(X)} p \circ f(x). \quad (3)$$

An interesting property of the Pareto front is as follows.

Lemma 1 (See [56]). *Assume p is monotonically increasing. We have*

$$\arg \min_{x \in X} p \circ f(x) = \arg \min_{x \in \mathcal{P}_f(X)} p \circ f(x). \quad (4)$$

In light of Lemma 1, as long as the user's preference function is monotonically increasing, it is sufficient to just evaluate the Pareto optimal architectures, in order to find the best one among all architectures.

One natural choice for a preference function is the weighted sum function. However, to apply the weighted sum preference function, different performance maps must share the same image set. Thus, the performance data of the Pareto optimal architectures are first normalized to \hat{f} using a re-scale function $r : \mathbb{R}^3 \rightarrow [0, 1]^3$, such that $\hat{f}(x) = r(f(x))$ with

$$\hat{f}_i(x) = r_i(f_i(x)) := \frac{f_i(x) - \underline{f}_i}{\bar{f}_i - \underline{f}_i}, \quad \forall x \in \mathcal{P}_f(X), \quad \forall i \in \{1, 2, 3\}, \quad (5)$$

where $\underline{f}_i = \min_{x \in \mathcal{P}_f(X)} f_i(x)$ and $\overline{f}_i = \max_{x \in \mathcal{P}_f(X)} f_i(x)$, and we assume $\underline{f}_i \neq \overline{f}_i$. In this case, the preference function has the form

$$p(f) = \sum_{i=1}^3 \lambda_i r_i(f_i) = \sum_{i=1}^3 \lambda_i \hat{f}_i, \quad (6)$$

with $\sum \lambda_i = 1$. In this example, each weight λ_i associated with \hat{f}_i indicates how much the user cares about criterion i .

Remark 1. *The re-scale function r_i is an increasing linear map on the performance data f_i for every $i \in \{1, 2, 3\}$. Applying this function on the performance data does not change the set of Pareto optimal solutions. Moreover, since the weighted sum function is also increasing with respect to the re-scaled performance data \hat{f} , Lemma 1 holds.*

3.4. Rediscovery of Architectures by Linear Programming

In this section, we explore the inverse direction of finding the best architecture.

Definition 3. *The rediscovery of architectures refers to identifying the specific preference function for a given Pareto optimal architecture under which it is optimal.*

We start by considering only the weighted sum preference function on the re-scaled data. Given a $x^* \in \mathcal{P}_f(X)$, identifying the weight $\lambda = (\lambda_1, \lambda_2, \lambda_3)$ can be formulated as a Linear Programming (LP) problem, of the form

$$\begin{aligned} & \min \lambda^T f(x^*) \\ & \text{s. t. } \begin{cases} \lambda^T f(x^*) \leq \lambda^T f(x), & \text{for every } x \in \mathcal{P}_f(X) \text{ and } x \neq x^* , \\ 0 \leq \lambda_i \leq 1 \text{ and } \sum_i \lambda_i = 1 . \end{cases} \end{aligned} \quad (7)$$

This LP problem can be easily solved using modern LP solvers, e.g., CPLEX [57].

4. First Application: Predicting glucose trajectory

Forecasting glucose trajectories based on continuous glucose monitors (CGM) data is necessary for improving diabetes management and maintaining optimal glycemic range. This example focuses

on designing the optimal architectures based on preference functions to forecast the glucose trajectory based on the CGM dataset provided in Ref. [58]. The raw dataset was provided in Ref. [59] which includes the CGM measurements from five patients, and was pre-processed in Ref. [58]. In this example, we analyze the glucose trajectory of the first patient. The total length of the signal is 2,125 time steps, in which the initial 1,650 time steps are used for training and validation. Forecasting is performed using a reference time point at the 1,650th time steps. Using a sliding window technique, the datasets include 1,377 training samples and 154 validation samples. For each sample, the lookback window is 96 time steps and the forecasting window is 24 time steps. With the time interval of 5 minutes, the forecasting horizon is 2 hour, which is a target time horizon for diabetes patients [60]. The models are trained on NVIDIA GeForce RTX 3090 and the implementation is in PyTorch [61].

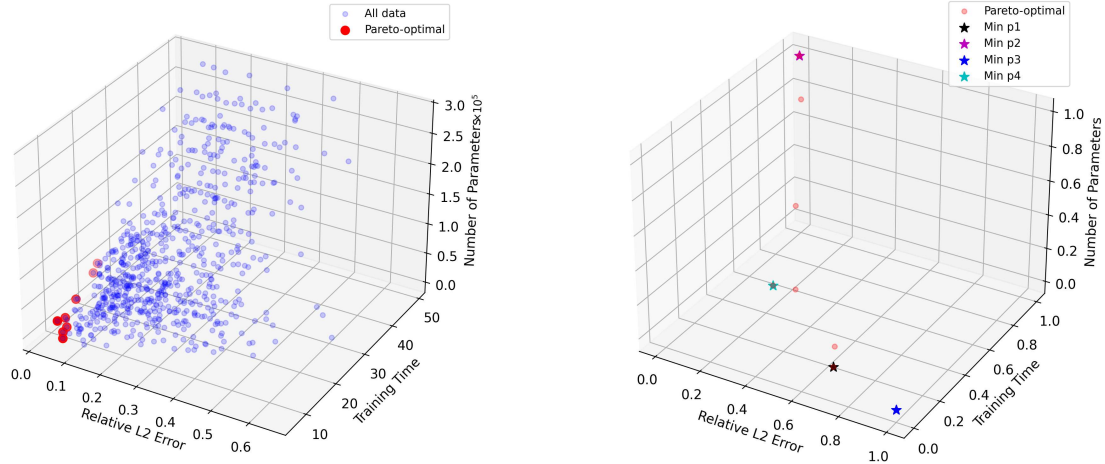
4.1. Construction of Architectures and Results of Pareto Optimal Front

In this application, we consider both the number and the sequence of each type of blocks in the construction of architectures. Moreover, we focus on some particular combinations in the construction, though the possible combinations are theoretically infinite. In particular, for the composite model, the vector $\mathbf{x}_1 = [n, m, j, k]$ represents the number of each type of blocks, where each element n, m, j, k can range from 0 to 2. To ensure valid configurations, the combination $\mathbf{x}_1 = [0, 0, 0, 0]$ is removed. Here, we introduce x_2 to represent the sequence of blocks, which is chosen from the set [1, 2, 3, 4, 5, 6]. When $x_2 = 1$, the sequence of blocks is [SSM, Attention, GRU, LSTM]. The detailed represented sequence corresponding to other numbers are shown in Table 1. The hidden dimension of each block x_3 is selected from [16, 32, 64]. This setup yields a total of 708 network architectures to predict the glucose trajectory. Among 708 different architectures, there are 8 Pareto optimal ones. Figure 2(a) presents the Pareto front, evaluating the relative \mathcal{L}_2 error f_1 , the total training time f_2 , and the number of parameters f_3 . In particular, the blue points in Figure 2(a) represent all the cases we considered, while the red points correspond to the Pareto optimal cases. This figure clearly shows that different performance criteria lead to different optimal architectures, and that no single architecture is optimal across all criteria. Moreover, we observe significant variation both among all the architectures and within the Pareto optimal ones, underscoring the necessity of the development

of tools to identify the optimal architecture.

Table 1: The number in x_2 represents different sequence of blocks.

x_2	Sequence of blocks
1	[SSM, Attention, GRU, LSTM]
2	[Attention, SSM, GRU, LSTM]
3	[SSM, GRU, Attention, LSTM]
4	[GRU, Attention, SSM, LSTM]
5	[Attention, GRU, SSM, LSTM]
6	[GRU, SSM, Attention, LSTM]



(a) Pareto front: all architectures are depicted in blue, while Pareto optimal architectures are highlighted in red.

(b) Discovery of optimal architecture: architectures selected by the preference functions are highlighted with star symbols and distinguished by different colors (normalized coordinates).

Figure 2: First Application: (a) Pareto front evaluating relative error–training time–number of parameters, and (b) discovery of optimal architectures using different preference functions for the glucose prediction.

4.2. Discovery of New Optimal Architectures

We apply the preference function-based approach presented in subsection 3.3 to discover the optimal architecture. In particular, we start with the weighted sum preference functions.

Preference function 1. $p^1(f) := 1/3\hat{f}_1 + 1/3\hat{f}_2 + 1/3\hat{f}_3$. This preference function represents an equally weighted sum of the three objectives. This formulation seeks a balanced compromise across all objectives, and each objective contributes equally to the overall result.

Preference function 2. $p^2(f) := \hat{f}_1$. This preference function is intended to find the optimal architectures, which obtains the smallest relative \mathcal{L}_2 error.

Preference function 3. $p^3(f) := \hat{f}_2$. This preference function is intended to find optimal architectures that require the least training time.

Preference function 4. $p^4(f) := 3/5\hat{f}_1 + 1/5\hat{f}_2 + 1/5\hat{f}_3$. This preference function greatly emphasizes the accuracy while still considering training time and the number of parameters.

We present the discovery of optimal architectures by these preference functions in Figure 2(b). In particular, we highlight with star symbols the selected optimal points, which correspond to the architecture that best matches the specified preference function. Note that the coordinates in Figure 2(b) are the normalized objective functions.

The preference function p^1 selects an architecture with one GRU block and one LSTM block, which achieves a moderate relative \mathcal{L}_2 error of 5.55%, a low training time of 7.746 s, while the number of parameters is 4,377. The preference function p^2 yields an architecture with the best accuracy with the relative \mathcal{L}_2 error of 2.89%, but it also requires the highest cost (21.331 s for training time and 52,793 parameters). This designed architecture includes a mix of two GRU blocks, one SSM block, one multi-head Attention block and one LSTM block. We also independently fine-tune the Transformer, which achieves the relative \mathcal{L}_2 error of 4.10%. The architecture corresponding to the preference function p^3 addresses efficiency, which chooses a configuration with a single-layer GRU, leading to the shortest training time (6.443 s). Finally, p^4 prioritizes accuracy while also taking training costs into consideration. The selected architecture includes one multi-head attention block and one GRU block. The optimal architectures and their performance are summarized in Table 2.

Table 2: First Application: The optimal architectures and their performance, selected by the preference functions p^1 , p^2 , p^3 and p^4 , for the glucose prediction.

Preference functions	Hidden dimension	Sequence and number of blocks	Relative \mathcal{L}_2 error f_1	Training time (s) f_2	Number of parameters f_3
p^1	16	[GRU=1, LSTM=1]	5.55%	7.746	4,377
p^2	32	[GRU=2, SSM=1, Attention=1, LSTM=1]	2.89%	21.331	52,793
p^3	16	[GRU=1]	6.77%	6.443	2,201
p^4	32	[Attention=1, GRU=1]	4.20%	9.945	15,673

4.3. Rediscovery of Existing Optimal Architectures

The discovery part illustrates that the optimal network architectures can be designed based on user-defined preference functions and provides ideal performance metrics. To rediscover the weighted sum preference functions for specific network architectures, we employ the Linear Programming method shown in [subsection 3.4](#). In [Table 3](#) we show four representative network architectures selected from the Pareto optimal ones. Each architecture presented in [Table 3](#) is the optimal one, under the particular weighted sum preference function with coefficients λ_1 , λ_2 and λ_3 . On the other hand, the coefficients also illustrate each architecture’s specific advantages. In particular, Cases 2 and 4 in [Table 3](#) represent composite architectures composed of various types of blocks. These cases identify significantly higher values for λ_1 compared to the other two coefficients, indicating that these architectures prioritize accuracy while maintaining lower training costs. Case 3 involves a single-layer GRU with a hidden dimension of 64, identifies a larger λ_2 and a smaller λ_1 . These values imply that this architecture addresses shorter training time and reduced accuracy, but does take into account the number of parameters.

Table 3: First Application: Optimal architectures rediscovered using the LP approach, along with the corresponding coefficients of the weighted sum preference functions for the glucose prediction.

Case	Hidden dimension	Sequence and number of block	Weights		
			λ_1	λ_2	λ_3
1	16	[Attention=1, LSTM=1]	0.383	0	0.617
2	32	[SSM=1, Attention=1, GRU=2]	0.697	0	0.303
3	64	[GRU=1]	0.048	0.952	0
4	32	[GRU=2, SSM=1, Attention=1, LSTM=1]	1	0	0

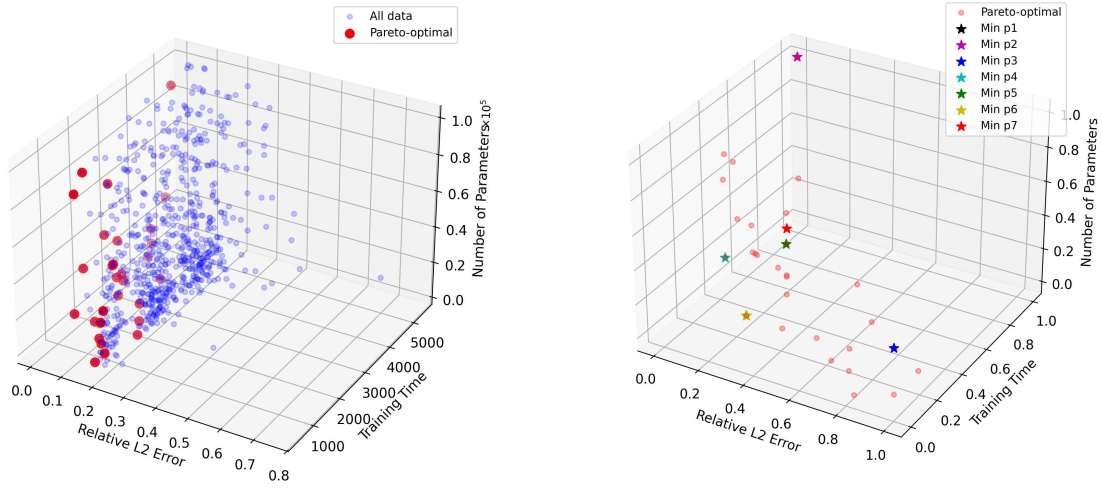
5. Second Application: Forecasting significant wave heights in Pelabuhan Ratu, Indonesia

ERA5 provides the global atmospheric reanalysis data from January 1940 to the present [62]. In this study, ERA5 hourly data on significant wave height (combined wind waves and swell) are used. The goal is to forecast the significant wave heights based on historical observations. For this example, the forecast is carried out with a reference time of January 25, 2020, at 01:00:00. The observations of the significant wave heights from January 1, 2014, at 00:00:00 to January 25, 2020, at 01:00:00 are used as the training data. For each sample, the lookback window is 648 time steps

(27 days) and the forecasting time is 72 time steps (3 days). The models for this example are trained on NVIDIA H100 GPU.

5.1. Construction of Architectures and Results of Pareto Optimal Front

The construction of architectures in this application is the same with the first application, which considers both the number and the sequence of each type of blocks. Each element of the vector \mathbf{x}_1 ranges from 0 to 2. The sequence of blocks x_2 are shown in Table 1. The hidden dimension of each block x_3 is selected from [8, 16, 32]. This setup yields a total of 708 network architectures to forecast the significant wave height. The Pareto front is presented in Figure 3(a), and there are 31 Pareto optimal architectures.



(a) Pareto front: all architectures are depicted in blue, while Pareto optimal architectures are highlighted in red.

(b) Discovery of optimal architecture: architectures selected by the preference functions are highlighted with star symbols and distinguished by different colors (normalized coordinates).

Figure 3: Second Application: (a) Pareto front evaluating relative error–training time–number of parameters, and (b) discovery of optimal architectures using different preference functions, for significant wave heights.

5.2. Discovery and Rediscovery of Optimal Architectures

To discover optimal architectures, we consider the four weighted sum preference function p^1, p^2, p^3, p^4 presented in subsection 4.2, and three new nonlinear preference functions. Note that, without loss of generality, we consider preference functions that may apply to the original data f or re-scaled data \hat{f} , where \hat{f} is obtained by applying an increasing linear map r on f .

Preference function 5. $p^5(f) := p_1^5(f_1) + \frac{1}{2}\hat{f}_2 + \frac{1}{2}\hat{f}_3$, where

$$p_1^5(f_1) = \begin{cases} 0, & f_1 \leq 0.06, \\ 10^3, & f_1 > 0.06. \end{cases} \quad (8)$$

This preference function emphasizes the importance of the model accuracy by maintaining a relative \mathcal{L}_2 error below 0.06 to avoid penalty. However, once accuracy is guaranteed, minimizing the computational cost (f_2 and f_3) becomes the critical factor.

Preference function 6. $p^6(f) := \hat{f}_1 + p_2^6(f_2) + p_3^6(f_3)$, where

$$p_2^6(f_2) = \begin{cases} 0, & f_2 \leq 1,000, \\ 10^3, & f_2 > 1,000, \end{cases} \quad (9)$$

and

$$p_3^6(f_3) = \begin{cases} 0, & f_3 \leq 35,000, \\ 10^3, & f_3 > 35,000. \end{cases} \quad (10)$$

This preference function imposes hard constraints on the computational costs, which limits the maximum training time to be 1,000 s, and the maximum number of parameters to be 35,000. Among the fast models, with values lower than these thresholds, the model accuracy is prioritized.

Preference function 7. $p^7(f) := 0.7\hat{f}_1 + 0.01 \log_2(f_2) + 0.01 \max(0, f_3 - 20,000)$. In this preference function, the model accuracy f_1 is heavily weighted to emphasize model performance. The penalty on the training time is reduced, and is represented by the logarithm of the training time. The number of parameters is penalized linearly when it exceeds 20,000.

We present the discovery of optimal architectures by the preference functions $\{p^i\}_{i \in \{1, \dots, 7\}}$ in [Figure 3\(b\)](#). The configurations of the designed network architecture and performance metrics are summarized in [Table 4](#). In this example, the preference function p^2 chooses the architecture with a mix of two attention blocks, two GRU blocks, two SSM blocks and one LSTM block, which achieves the lowest relative \mathcal{L}_2 error of 1.35%. The one single-layer LSTM uses the least training time, but has a highest relative \mathcal{L}_2 error of 20.79%. The nonlinear preference function p^5 selects architectures

with one SSM layer, two Attention layers and two GRU layers, which achieves the relative \mathcal{L}_2 error below 6%. The p^6 chooses the same architecture with p^1 . Compared to Table 2 and Table 4, the designed architectures in Table 4 are more complex than those in Table 2, likely due to the increased complexity of the climate problem.

Table 5 presents the rediscovery results, which aim to determine the best coefficients for preference functions across six specific network architectures. These coefficients highlight the advantages of each architecture. In particular, the most complex architectures, which involves all four types of blocks in Cases 2 and 5, exhibit the highest λ_1 values, indicating that these architectures prioritize higher accuracy. In contrast, the simplest architecture, Case 1, consisting of two SSM blocks and one LSTM block, identifies a larger λ_2 and a moderate λ_1 , which emphasize shorter training time while maintaining a focus on accuracy.

Table 4: The optimal architectures and their performance, selected by the preference functions $p^1 - p^7$, for significant wave heights.

Preference functions	Hidden dimension	Sequence and number of blocks	Relative \mathcal{L}_2 error f_1	Training time (s) f_2	Number of parameters f_3
p^1	16	[SSM=1, GRU=1]	7.54%	836.216	19,208
p^2	32	[Attention=2, GRU=2, SSM=2, LSTM=1]	1.35%	5021.512	90,952
p^3	32	[LSTM=1]	20.79%	434.232	33,608
p^4	16	[SSM=2, GRU=1, LSTM=2]	3.89%	1540.144	33,128
p^5	8	[SSM=1, Attention=2, GRU=2]	3.09%	3889.595	8,152
p^6	16	[SSM=1, GRU=1]	7.54%	836.216	19,208
p^7	16	[GRU=2, Attention=2, LSTM=1]	2.68%	4074.706	13,448

Table 5: Second Application: Optimal architectures rediscovered using the LP approach, along with the corresponding coefficients of the weighted sum preference functions for significant wave heights.

Case	Hidden dimension	Sequence and number of block	Weights		
			λ_1	λ_2	λ_3
1	32	[SSM=2, LSTM=1]	0.368	0.632	0
2	16	[SSM=2, Attention=1, GRU=1, LSTM=1]	0.781	0.098	0.121
3	16	[SSM=2, GRU=1, LSTM=2]	0.686	0.314	0
4	8	[SSM=1, Attention=1, GRU=2]	0.148	0.090	0.762
5	16	[Attention=2, SSM=2, GRU=2, LSTM=1]	0.920	0	0.08
6	16	[SSM=1, GRU=2, Attention=1]	0.713	0.127	0.160

6. Third Application: Predicting Vortex-Induced Vibrations (VIV) of Marine Risers

The Norwegian Deepwater Programme (NDP) conducted VIV tests on a 38 m long riser in 2003, which provided extensive data at various current speeds and profiles. The bending strain and accelerations along the riser in both in-line and cross-flow directions were measured. In this study, we focus on the cross-flow strain recorded by the 10th strain gauge under a uniform flow with a speed 0.7 m/s. The total length of the signal is 156,600 time steps. The stationary part with the 30,000 time steps is chosen in this example, in which the first 27,000 time steps are used for training and validation. The goal of this example is to forecast 60 time steps from the current time defined at 27,000 s. A sliding window technique is applied by using a window length of 1,000 time steps each example with a shift interval of 5 time steps, which results in 5,201 samples in total. Here, 90% of these samples are chosen as the training samples and the rest are used for validation. For each sample, the lookback window is 900 time steps. The models for this example are trained on NVIDIA RTX A6000.

6.1. Construction of Architectures and Results of Pareto Optimal Front

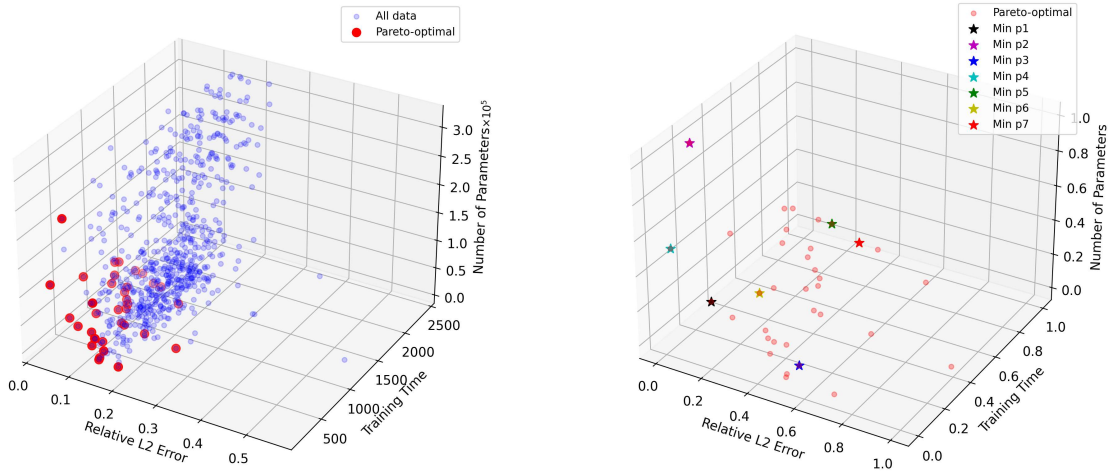
The construction of architectures in this application is the same with the first two applications, which considers both the number and the sequence of each type of blocks. Each element of the vector \mathbf{x}_1 ranges from 0 to 2. The sequence of blocks x_2 are shown in [Table 1](#). The hidden dimension of each block x_3 is selected from [16, 32, 64]. This setup yields a total of 708 network architectures to forecast the motion of the riser. The Pareto front is presented in [Figure 4\(a\)](#), and there are 35 Pareto optimal architectures.

6.2. Discovery and Rediscovery of Optimal Architectures

To discover optimal architectures, we consider the four weighted sum preference function p^1, p^2, p^3, p^4 presented in [subsection 4.2](#), and the three nonlinear preference functions p^5, p^6, p^7 presented in [subsection 5.2](#).

We present the optimal architectures discovered by these preference function in the Pareto front in [Figure 4\(b\)](#). The network architectures and performance metrics are also summarized in [Table 6](#). Moreover, we present detailed illustrations of the second modules of the designed architectures in

Figure 5. The first and third modules are the same across all cases, which are shown in Figure 1. The GRU with one-single layer is the fastest. The architecture with one SSM block and two LSTM blocks achieves the highest accuracy of 2.99%, which is different from the architectures which achieve the highest accuracy in the other two examples (see the second rows in Table 2 and Table 4). The nonlinear preference function p^5 has a threshold of relative \mathcal{L}_2 error equals 6%, which finds the architecture with two Attention blocks first, followed by one SSM block, one GRU block and one LSTM block (see Figure 5(e)). Here, p^6 has thresholds for the training time and the number of parameters to ensure the computational efficiency. The resulting architecture includes a sequence starting with one GRU block, followed by two SSM blocks, and concluding with two LSTM blocks (see Figure 5(f)). As shown in Figure 5(g), the designed architecture for p^7 consists of a sequence starting with two GRU blocks, followed by two Attention blocks and two LSTM blocks to guarantee the computational accuracy and computational costs. Table 7 shows the best coefficients of preference functions for six specific network architectures. Each architecture identifies the corresponding best coefficients, which demonstrates their advantages.



(a) Pareto front: all architectures are depicted in blue, while Pareto optimal architectures are highlighted in red.

(b) Discovery of optimal architecture: architectures selected by the preference functions are highlighted with star symbols and distinguished by different colors (normalized coordinates).

Figure 4: Third Application: (a) Pareto front evaluating relative error–training time–number of parameters, and (b) discovery of optimal architectures using different preference functions, for VIV of the marine risers.

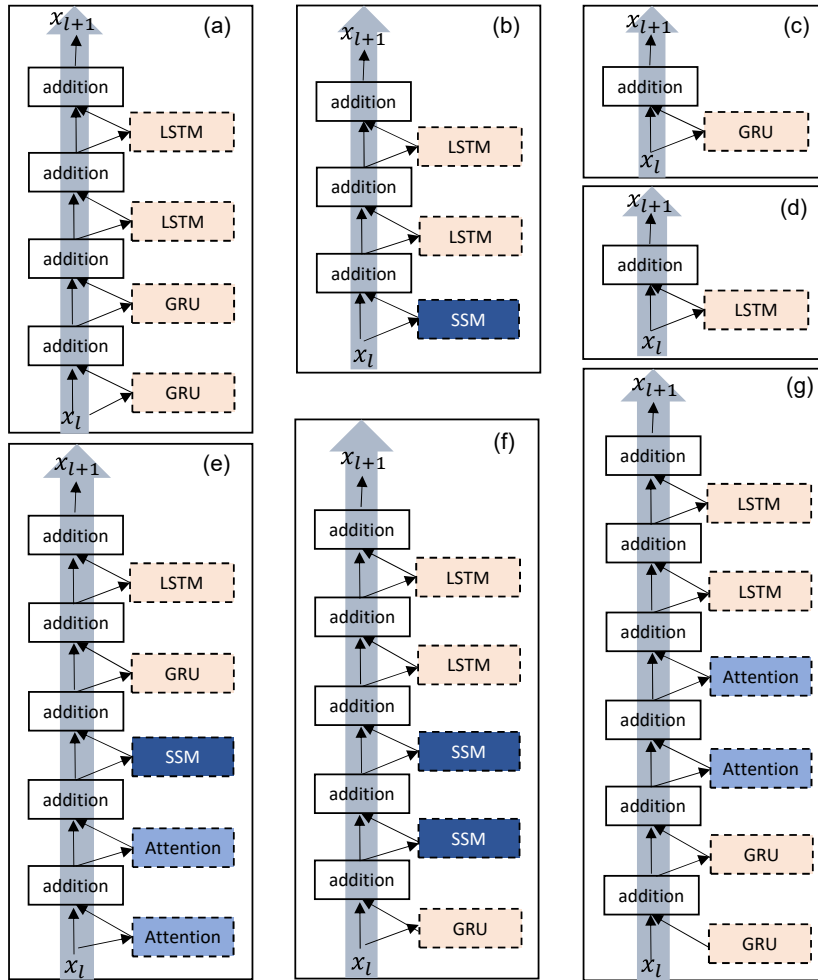


Figure 5: Third Application: Designed network architectures for marine risers based on given preference functions: (a) p^1 , (b) p^2 , (c) p^3 , (d) p^4 , (e) p^5 , (f) p^6 , (g) p^7 .

Table 6: Third Application: The optimal architectures and their performance, selected by the preference functions $p^1 - p^7$, for VIV of the marine riser.

Preference functions	Hidden dimension	Sequence and number of blocks	Relative \mathcal{L}_2 error f_1	Training time (s) f_2	Number of parameters f_3
p^1	32	[GRU=2, LSTM=2]	6.18%	284.913	52,847
p^2	64	[SSM=1, LSTM=2]	2.99%	421.400	207,439
p^3	32	[GRU=1]	15.84%	162.964	29,615
p^4	64	[LSTM=1]	3.68%	171.634	116,687
p^5	16	[Attention=2, SSM=1, GRU=1, LSTM=1]	5.88%	1450.476	20,415
p^6	16	[GRU=1, SSM=2, LSTM=2]	7.39%	605.517	32,159
p^7	16	[GRU=2, Attention=2, LSTM=2]	9.23%	1395.611	14,655

Table 7: Third Application: Optimal architectures rediscovered using the LP approach, along with the corresponding coefficients of the weighted sum preference functions for VIV of the marine riser.

Case	Hidden dimension	Sequence and number of block	Weights		
			λ_1	λ_2	λ_3
1	16	[SSM=1, LSTM=1]	0.259	0.076	0.665
2	32	[Attention=2, LSTM=1]	0.851	0	0.149
3	32	[GRU=2, LSTM=2]	0.253	0.515	0.232
4	16	[Attention=1, GRU=2]	0.142	0	0.858
5	16	[Attention=2, SSM=1, GRU=1, LSTM=1]	0.173	0	0.827
6	16	[GRU=1, SSM=2, LSTM=2]	0.352	0.087	0.561

7. Fourth Application: Predicting the Motions of Floating Offshore Structures

In this section, we consider a simulation example introduced in [22]. This example studies a semi-submersible platform with the mooring system, which is plotted in Figure 6. The platform weighs 53.4×10^3 tons, with a length of 105 m and a working water depth of 234 m. The four sets of mooring lines are evenly spaced, each at a 90° angle. Within each set, the angle between two mooring lines is 50° . The mooring line is chain-type with the total length of 1,700 m and the diameter of 158.76 mm. Its mass per unit length is 154.53 kg/m, the axial stiffness is 712.7 kN and the breaking strength is 7200 kN. The added mass coefficient, the inertia coefficient and the drag coefficient are 1, 0.07 and 1, respectively. For further details, the reader is referred to Ref. [22].

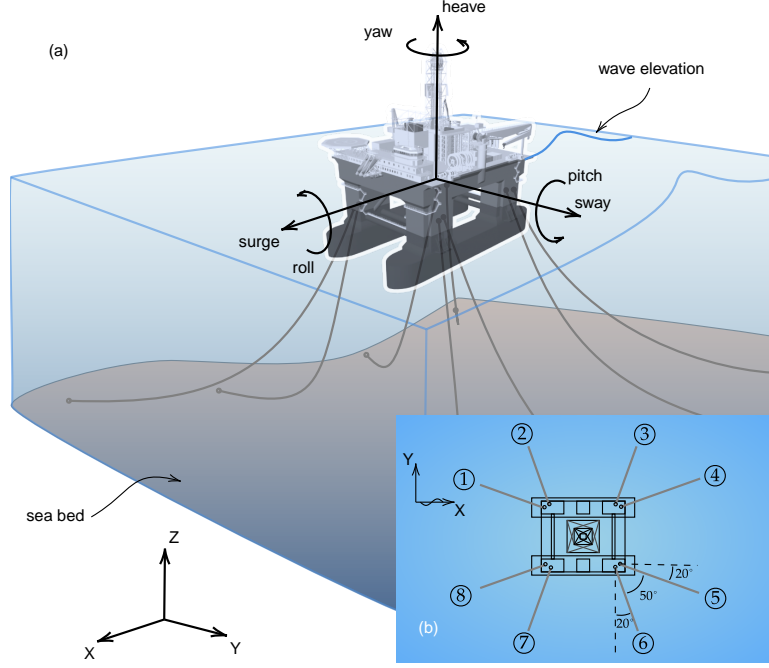


Figure 6: A schematic representation of a semi-submersible platform with the mooring system: (a) side view, (b) top view [22].

The platform is modeled as a rigid body with six degrees of freedom (DOF) involving three translational and three rotational motions. The equation of motion is written as [63]

$$(\mathbf{M} + \mathbf{A})\ddot{\mathbf{x}}(t) + \int_0^t \mathbf{K}(t - \tau)\dot{\mathbf{x}}(\tau)d\tau + \mathbf{C}\mathbf{x}(t) + \mathbf{f}_{moor}(\mathbf{x}(t), \dot{\mathbf{x}}(t)) = \mathbf{f}_{wa}(\eta(t)) , \quad (11)$$

where $\ddot{\mathbf{x}}(t)$, $\dot{\mathbf{x}}(t)$ and $\mathbf{x}(t) \in \mathbb{R}^{6 \times 1}$ are the acceleration, velocity, and displacement of the floating structure, respectively; \mathbf{M} , \mathbf{A} and $\mathbf{C} \in \mathbb{R}^{6 \times 6}$ are the body mass, constant added mass, and the linearized hydrostatic restoring force coefficient, respectively; $\mathbf{K}(t)$ is the retardation function. The mooring force $\mathbf{f}_{moor}(\mathbf{x}(t), \dot{\mathbf{x}}(t)) \in \mathbb{R}^{6 \times 1}$ is a nonlinear function of the motions of the platform. The wave force $\mathbf{f}_{wa}(\eta(t)) \in \mathbb{R}^{6 \times 1}$ is related to the incident wave elevation $\eta(t)$, which is computed by carrying out a diffraction analysis [64, 65]. The JONSWAP spectrum with the significant wave height, $H_s = 3.5$ m, and zero-crossing wave period, $T_z = 8.5$ s, is chosen to generate the realizations of wave elevations. The heading angle of the wave is 0° . After generating the hydrodynamic data by WAMIT [66], the motion of the platform in Figure 6 is obtained by running a commercial software. Typically, the surge, heave and pitch are the most dominant motions for this wave approach condition, so here we only consider heave and surge.

The aim of this example is to forecast the motion based on the historical data. To train the proposed composite model, we conduct a simulation lasting about 3 hours on a single CPU. The data collected from the beginning of the simulation (0 s) to 10,373 s are used for training and validation. The forecasting time is 12 s from the current time (10,373 s). We further apply a sliding window technique by using a window length of 1,000 time steps per sample with a shift interval of 10 time steps. This process yields 5,100 samples and each comprises 1,000 time steps. The time interval is 0.2 s. For model training, 90% of these samples are randomly chosen, while the remaining 10% are allocated for validation. The models are trained on NVIDIA GeForce RTX 3090.

7.1. Heave Motion

As shown in [Figure 6](#), heave motion refers to the vertical motion along the vertical axis (z) of the platform. This example aims to forecast the heave motion of the platform.

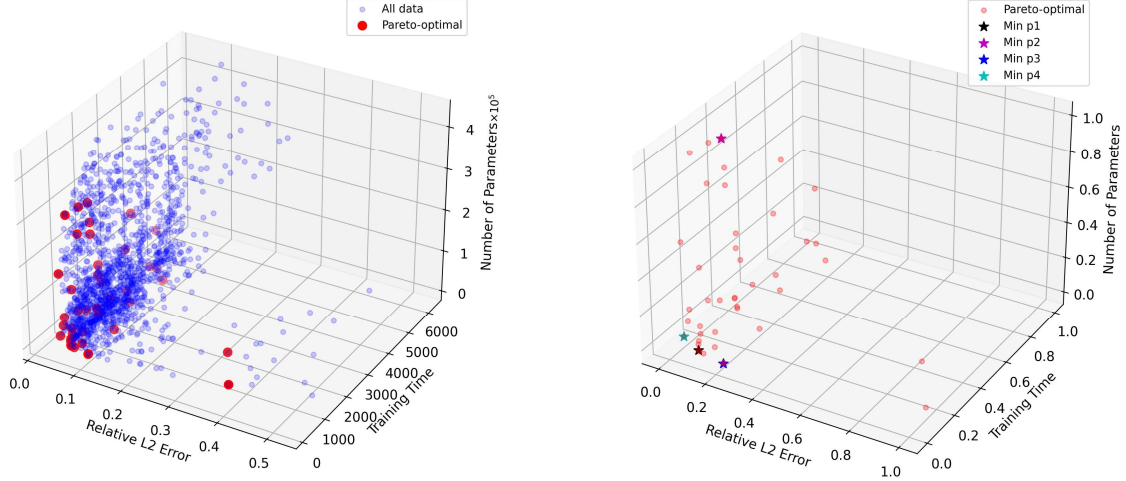
7.1.1. Results of Pareto Optimal Architectures

In this example, only the number of each type of blocks is considered. We extend the range of each element in the vector \mathbf{x}_1 from 0 – 2 to 0 – 3. To ensure valid configurations, the combination $\mathbf{x}_1 = [0, 0, 0, 0]$ is removed, resulting in a total of 255 network architectures. The sequence of blocks is fixed to [SSM, Attention, GRU, LSTM]. The lookback window, represented by x_3 , is selected from the set [500, 900], and the hidden dimension, x_4 , is chosen from [16, 32, 64]. The down-sampling is fixed to 2. This setup yields a total of 1,530 cases to forecast the heave motion of the platform. In this example, among 1,530 different architectures, there are 43 Pareto optimal ones. In [Figure 7\(a\)](#), we present the Pareto front.

7.1.2. Discovery and Rediscovery of Optimal Architectures

To discover optimal architectures, the four weighted sum preference function p^1, p^2, p^3, p^4 presented in [subsection 4.2](#) are used. [Table 8](#) summarizes the designed network architectures performance metrics. Compared to [Table 2](#), [Table 6](#) with [Table 8](#), we find out the designed architectures with the same preference functions are very different for different problems.

One interesting direction to study is to compare our best-performing model and the LSTM fine-tuned using Optuna [\[67\]](#), which is an open-source hyperparameter optimization framework that can



(a) Pareto front: all architectures are depicted in blue, while Pareto optimal architectures are highlighted in red

(b) Discovery of optimal architectures: architectures selected by the preference functions are highlighted with star symbols and distinguished by different colors (normalized coordinates).

Figure 7: Fourth Application: (a) Pareto front evaluating relative error–training time–number of parameters, and (b) discovery of optimal architectures using different preference functions for heave motion.

Table 8: Fourth Application: The optimal architectures and their performance, selected by the preference functions p^1 , p^2 , p^3 and p^4 , for the heave motion of the platform.

Preference functions	Lookback window	Hidden dimension	Block: {GRU, LSTM, multi-head Attention, SSM}	Relative \mathcal{L}_2 error f_1	Training time (s) f_2	Number of parameters f_3
p^1	900	16	[2, 0, 0, 0]	6.59%	268.241	10,558
p^2	500	64	[1, 3, 2, 1]	2.66%	1,827.576	266,654
p^3	900	16	[1, 0, 0, 0]	10.85%	166.836	8,926
p^4	500	32	[1, 0, 0, 0]	4.79%	197.642	30,110

automate the process of searching for the best hyperparameters. Table 9 summarizes the search space for each hyperparameter for both Optuna and our method, which shows the search spaces of Optuna are much larger than our method. The chosen hyperparameters and evaluation metrics are summarized in Table 10. The “Optuna (LSTM)” represents the traditional LSTM model, while “Optuna (LSTM with Embedding)” includes a linear transformation to lift the input to a higher dimensional space before feeding it into the LSTM layer. As we seen from Table 10, the fine-tuned LSTM with embedding optimized by Optuna obtains the lowest error among all LSTM training. However, its error is still higher than that of our best model determined by the preference function p^2 . The LSTM trained with our method shows a slightly higher error than the others, but the computational cost is the lowest. Table 11 shows the rediscovery results, which aims to find the best coefficients of prefer-

ence functions for five specific network architectures. The advantages of these network architectures are demonstrated by these coefficients.

Table 9: Fourth Application: Comparison of hyperparameter search spaces for LSTM.

	Our method for LSTM	Optuna for LSTM
Hidden dimension	[16, 32, 64]	[16, 32, 48, 64, 96, 128]
Number of layers	0 to 3	1 to 5
Learning rate	1e-3	1e-5 to 1e-1
Batch size	50	16 to 128

Table 10: Fourth Application: Comparison of hyperparameters and evaluation metrics for LSTM Training.

	Hidden dimension	Number of layers	Learning rate	Batch size	Relative \mathcal{L}_2 error	Training time	Number of parameters
Our method (LSTM)	32	1	1e-3	50	7.19%	174.255	32,222
Optuna (LSTM)	128	3	1.84e-3	45	6.07%	1017.050	335,134
Optuna (LSTM with Embedding)	128	5	5.55e-3	107	4.37%	1413.005	664,606
Our method (best)	64	[GRU=1, LSTM=3, Attention=2, SSM=1]	1e-3	50	2.66%	1827.576	266,654

Table 11: Fourth Application: Optimal architectures rediscovered using the LP approach, along with the corresponding coefficients of the weighted sum preference functions, for the heave motion of the platform.

Case	Lookback window	Hidden dimension	Block: {GRU, LSTM, Attention, SSM}	Weights		
				λ_1	λ_2	λ_3
1	500	32	[1, 0, 0, 0]	0.073	0.927	0
2	900	32	[0, 1, 0, 0]	0.016	0.984	0
3	900	32	[0, 0, 2, 3]	0.972	0	0.028
4	500	32	[1, 1, 0, 1]	0.882	0.073	0.045
5	900	16	[1, 3, 3, 0]	0.278	0	0.722

7.2. Surge Motion

In this section, we study the optimal network architectures that forecast the surge motion of the platform, which refers to the horizontal motion along the longitudinal axis (x) of the platform.

7.2.1. Results of Pareto Optimal Architectures

Similar to the setup of the composite model for the heave motion, each element of the vector \mathbf{x}_1 can range from 0 to 3 and the combination $\mathbf{x}_1 = [0, 0, 0, 0]$ is removed, which results in a total of 255 network architectures. The sequence of blocks is fixed to [SSM, Attention, GRU, LSTM]. The lookback window x_3 is selected from the set [500, 900], and the hidden dimension x_4 is chosen from [16, 32, 64]. Finally, a total of 1,530 architectures are set up. Among 1,530 architectures, there are 30 Pareto optimal ones. We present the Pareto front in [Figure 8\(a\)](#). We observe a similar behavior, both among all the architectures and within the Pareto optimal ones, as in heave motion. In particular, the proportion of Pareto-optimal solutions is lower in the surge motion case, suggesting greater variation among the architectures.

7.2.2. Discovery and Rediscovery of Optimal Architectures

For the surge motion, four weighted sum preference function p^1, p^2, p^3, p^4 introduced in [subsection 4.2](#) and three nonlinear preference functions are considered in this example. The nonlinear preference functions p^8, p^9, p^{10} have the similar forms as p^5, p^6, p^7 , but the threshold values of the evaluation metrics are changed.

Preference function 8. $p^8(f) := p_1^8(f_1) + \frac{1}{2}\hat{f}_2 + \frac{1}{2}\hat{f}_3$, where

$$p_1^8(f_1) = \begin{cases} 0, & f_1 \leq 0.04, \\ 10^3, & f_1 > 0.04. \end{cases} \quad (12)$$

This preference function has a similar form as $p^5(f)$. Here, we change the threshold values on the evaluation of the relative error.

Preference function 9. $p^9(f) = \hat{f}_1 + p_2^9(f_2) + p_3^9(f_3)$, where

$$p_2^9(f_2) = \begin{cases} 0, & f_2 \leq 500, \\ 10^3, & f_2 > 500. \end{cases} \quad (13)$$

and

$$p_3^9(f_3) = \begin{cases} 0, & f_3 \leq 35,000, \\ 10^3, & f_3 > 35,000, \end{cases} \quad (14)$$

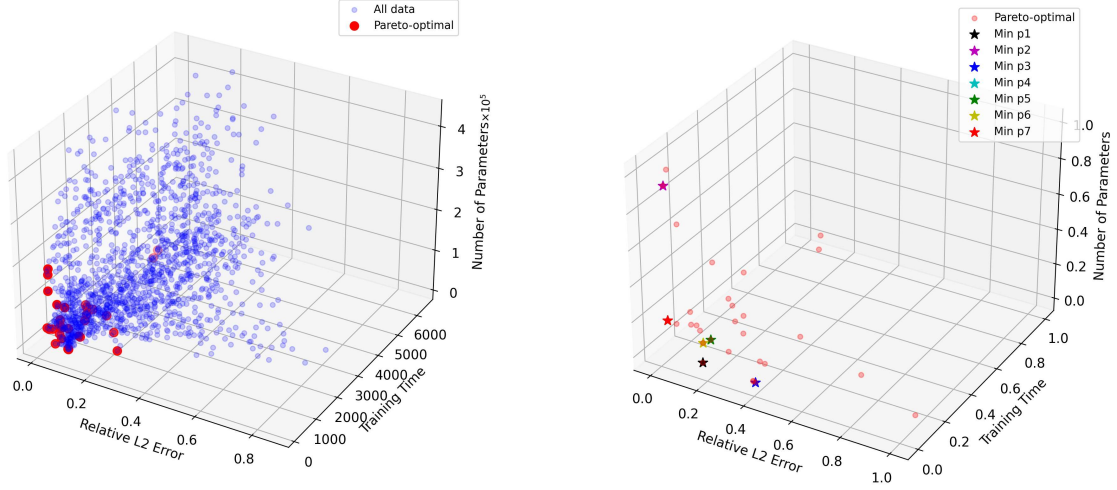
This preference function has a similar form as $p^6(f)$. Here, we change the threshold values on the evaluation of the training time and the number of parameters.

Preference function 10. $p^{10}(f) := 0.7\hat{f}_1 + 0.001 \max(0, f_2 - 500) + 0.01 \log_2(f_3)$. In this preference function, the model accuracy f_1 is heavily weighted to emphasize model performance. The training time f_2 is also linearly penalized when the training time exceeds 500 s, which means the penalty linearly grows with the increase of the training time. To reduce the penalty's impact on larger models, the model complexity f_3 is represented by the logarithm of the number of parameters.

Figure 8(b) plots the discovery of optimal architectures by the preference functions. The configurations of the designed network architecture and performance metrics are summarized in Table 12. We apply the Linear Programming method presented in subsection 3.4 to rediscover the optimal architectures, for weighted sum preference functions. Table 13 shows five network architectures chosen from the Pareto optimal solutions, and we identify their best coefficients of preference functions. The network architectures designed for the above four applications are tailored to the specific data used, the assumed reference time (considered as the current time), and the selected preference function. Adjustments to any of these factors may find different optimal architectures, which further shows the importance of employing multi-objective optimization methods to address varying requirements.

Table 12: Fourth Application: The optimal architectures and their performance, selected by the preference functions $p^1 - p^4$ and $p^8 - p^{10}$, for the surge motion of the platform.

Preference functions	Lookback window	Hidden dimension	Block: {GRU, LSTM, multi-head Attention, SSM}	Relative \mathcal{L}_2 error f_1	Training time (s) f_2	Number of parameters f_3
p^1	500	16	[2, 0, 0, 0]	5.07%	228.318	10,558
p^2	900	64	[3, 0, 0, 0]	1.02%	458.642	159,262
p^3	500	16	[1, 0, 0, 0]	10.26%	197.457	8,926
p^4	900	32	[1, 1, 0, 0]	1.50%	296.125	38,558
p^8	500	16	[1, 1, 1, 0]	3.75%	909.489	11,102
p^9	900	16	[1, 1, 0, 1]	4.33%	484.437	20,670
p^{10}	900	32	[1, 1, 0, 0]	1.50%	296.125	38,558



(a) Pareto front: all architectures are depicted in blue, while Pareto optimal architectures are highlighted in red.

(b) Discovery of optimal architecture: architectures selected by the preference functions are highlighted with star symbols and distinguished by different colors (normalized coordinates).

Figure 8: Fourth Application: Pareto front evaluating relative error–training time–number of parameters, and discovery of optimal architectures using different preference functions for surge motion.

Table 13: Fourth Application: Optimal architectures rediscovered using the LP approach, along with the corresponding coefficients of the weighted sum preference functions, for the surge motion of the platform.

Case	Lookback window	Hidden dimension	Block: {GRU, LSTM, Attention, SSM}	Weights		
				λ_1	λ_2	λ_3
1	500	32	[1, 0, 0, 0]	0.011	0.989	0
2	900	32	[1, 1, 0, 0]	0.169	0.831	0
3	500	32	[1, 1, 0, 0]	0.092	0.898	0.010
4	900	16	[0, 1, 1, 0]	0.131	0.041	0.828
5	900	16	[1, 2, 3, 0]	0.575	0	0.425

8. Summary and Concluding Remarks

In this work, we proposed a general framework to automatically discover composite neural architectures, which integrate GRU, LSTM, multi-head Attention and SSM blocks. For benchmarks, we considered four diverse real-world applications, from biomedicine, weather, and flow-structure interactions. Compared with traditional models, which have a fixed architecture, the proposed model is more flexible. The number and sequence of each block are designed by using the multi-objective optimization approach to satisfy specific engineering needs and target objectives. As an inverse direction of designing the best network architecture, the particular preference function for a given Pareto optimal network architecture was also identified by the Linear Programming method. Four

practical problems were studied, and both linear and nonlinear preference functions were investigated. Several interesting phenomena were observed based on our results. If only the lowest training time was considered, a single-layer GRU or LSTM was always the best architecture. When focusing on the lowest relative \mathcal{L}_2 error or other combined evaluation objectives, the optimal architecture appeared to be data-dependent. Note that our contributions do not only come from introducing a novel composite model but rather from proposing an important multi-objective optimization method to evaluate and design network architectures based on the preference function. Taken together, our results explain why the literature presents different conclusions about the performance of different models that are based on fixed neural architectures.

In our experiments, however, we observed a significant offline computational cost in completing the training of all architectures for discovering and rediscovering the optimal architecture. We also observed that this offline computational cost is primarily due to the training procedure for non-Pareto optimal architectures, which take the majority (around 95%) of total architectures being constructed. Thus, for real-time applications, one interesting direction for future work is to develop an efficient sampling method, in the parameterized space of architectures, that will reduce significantly the total number of architectures while preserving the Pareto-optimal ones.

Acknowledgments

We would like to acknowledge support by the DARPA-DIAL grant HR00112490484, MURI-AFOSR FA9550-20-1-0358 project, and support from Shell, ExxonMobil, ABS, and Subsea 7.

References

- [1] E. Parzen, Ararma models for time series analysis and forecasting, *Journal of Forecasting* 1 (1) (1982) 67–82.
- [2] B. K. Nelson, Time series analysis using autoregressive integrated moving average (arima) models, *Academic Emergency Medicine* 5 (7) (1998) 739–744.
- [3] C. Meek, D. M. Chickering, D. Heckerman, Autoregressive tree models for time-series analy-

- sis, in: Proceedings of the 2002 SIAM International Conference on Data Mining, SIAM, 2002, pp. 229–244.
- [4] K.-j. Kim, Financial time series forecasting using support vector machines, *Neurocomputing* 55 (1-2) (2003) 307–319.
- [5] Y. Kim, J.-H. Kim, Y. Kim, Time series prediction of nonlinear ship structural responses in irregular seaways using a third-order volterra model, *Journal of Fluids and Structures* 49 (2014) 322–337.
- [6] S. Araghinejad, S. Araghinejad, *Time Series Modeling*, Springer, 2014.
- [7] J. Kaur, K. S. Parmar, S. Singh, Autoregressive models in environmental forecasting time series: a theoretical and application review, *Environmental Science and Pollution Research* 30 (8) (2023) 19617–19641.
- [8] T. Wu, H. Yang, P. Wang, C. Zhang, M. Zhang, Data-driven fatigue reliability evaluation of offshore wind turbines under floating ice loading, *Journal of Structural Engineering* 150 (12) (2024) 05024004.
- [9] G. P. Zhang, Time series forecasting using a hybrid arima and neural network model, *Neurocomputing* 50 (2003) 159–175.
- [10] C. Deb, F. Zhang, J. Yang, S. E. Lee, K. W. Shah, A review on time series forecasting techniques for building energy consumption, *Renewable and Sustainable Energy Reviews* 74 (2017) 902–924.
- [11] B. Lim, S. Zohren, Time-series forecasting with deep learning: a survey, *Philosophical Transactions of the Royal Society A* 379 (2194) (2021) 20200209.
- [12] J. F. Torres, D. Hadjout, A. Sebaa, F. Martínez-Álvarez, A. Troncoso, Deep learning for time series forecasting: a survey, *Big Data* 9 (1) (2021) 3–21.
- [13] Q. Cao, S. Goswami, G. E. Karniadakis, Laplace neural operator for solving differential equations, *Nature Machine Intelligence* 6 (6) (2024) 631–640.

- [14] S. Hochreiter, Long short-term memory, Neural Computation MIT-Press (1997).
- [15] A. Graves, J. Schmidhuber, Framewise phoneme classification with bidirectional lstm and other neural network architectures, Neural Networks 18 (5-6) (2005) 602–610.
- [16] S. Siami-Namini, N. Tavakoli, A. S. Namin, The performance of lstm and bilstm in forecasting time series, in: 2019 IEEE International conference on big data (Big Data), IEEE, 2019, pp. 3285–3292.
- [17] J. Y. Choi, B. Lee, Combining lstm network ensemble via adaptive weighting for improved time series forecasting, Mathematical Problems in Engineering (1) (2018) 2470171.
- [18] B. B. Sahoo, R. Jha, A. Singh, D. Kumar, Long short-term memory (lstm) recurrent neural network for low-flow hydrological time series forecasting, Acta Geophysica 67 (5) (2019) 1471–1481.
- [19] G. Makridis, D. Kyriazis, S. Plitsos, Predictive maintenance leveraging machine learning for time-series forecasting in the maritime industry, in: 2020 IEEE 23rd international conference on intelligent transportation systems (ITSC), IEEE, 2020, pp. 1–8.
- [20] S.-T. Tsai, E.-J. Kuo, P. Tiwary, Learning molecular dynamics with simple language model built upon long short-term memory neural network, Nature Communications 11 (1) (2020) 5115.
- [21] G. Tang, J. Lei, C. Shao, X. Hu, W. Cao, S. Men, Short-term prediction in vessel heave motion based on improved lstm model, IEEE Access 9 (2021) 58067–58078.
- [22] Q. Cao, S. Goswami, T. Tripura, S. Chakraborty, G. E. Karniadakis, Deep neural operators can predict the real-time response of floating offshore structures under irregular waves, Computers & Structures 291 (2024) 107228.
- [23] K. Cho, B. Van Merriënboer, C. Gulcehre, D. Bahdanau, F. Bougares, H. Schwenk, Y. Bengio, Learning phrase representations using rnn encoder-decoder for statistical machine translation. arxiv 2014, arXiv preprint arXiv:1406.1078 (2020).

- [24] J. Chung, C. Gulcehre, K. Cho, Y. Bengio, Empirical evaluation of gated recurrent neural networks on sequence modeling, arXiv preprint arXiv:1412.3555 (2014).
- [25] Y. Tang, J. Fan, X. Li, J. Ma, M. Qi, C. Yu, W. Gao, Physics-informed recurrent neural network for time dynamics in optical resonances, *Nature Computational Science* 2 (3) (2022) 169–178.
- [26] H. S. Heidenreich, P. R. Vlachas, P. Koumoutsakos, Deconstructing recurrence, attention, and gating: Investigating the transferability of transformers and gated recurrent neural networks in forecasting of dynamical systems, arXiv preprint arXiv:2410.02654 (2024).
- [27] P. R. Vlachas, J. Pathak, B. R. Hunt, T. P. Sapsis, M. Girvan, E. Ott, P. Koumoutsakos, Forecasting of spatio-temporal chaotic dynamics with recurrent neural networks: a comparative study of reservoir computing and backpropagation algorithms, arXiv preprint arXiv:1910.05266 42 (2019).
- [28] A. Vaswani, Attention is all you need, *Advances in Neural Information Processing Systems* (2017).
- [29] N. Wu, B. Green, X. Ben, S. O'Banion, Deep transformer models for time series forecasting: The influenza prevalence case, arXiv preprint arXiv:2001.08317 (2020).
- [30] Q. Wen, T. Zhou, C. Zhang, W. Chen, Z. Ma, J. Yan, L. Sun, Transformers in time series: A survey, arXiv preprint arXiv:2202.07125 (2022).
- [31] K. T. Chitty-Venkata, M. Emani, V. Vishwanath, A. K. Somani, Neural architecture search for transformers: A survey, *IEEE Access* 10 (2022) 108374–108412.
- [32] S. Khan, M. Naseer, M. Hayat, S. W. Zamir, F. S. Khan, M. Shah, Transformers in vision: A survey, *ACM computing surveys (CSUR)* 54 (10s) (2022) 1–41.
- [33] S. Islam, H. Elmekki, A. Elsebai, J. Bentahar, N. Drawel, G. Rjoub, W. Pedrycz, A comprehensive survey on applications of transformers for deep learning tasks, *Expert Systems with Applications* (2023) 122666.

- [34] A. J. Varghese, A. Bora, M. Xu, G. E. Karniadakis, Transformer_g2g: Adaptive time-stepping for learning temporal graph embeddings using transformers, *Neural Networks* 172 (2024) 106086.
- [35] Q. Chen, C. Cai, Y. Chen, X. Zhou, D. Zhang, Y. Peng, Tempronet: A transformer-based deep learning model for seawater temperature prediction, *Ocean Engineering* 293 (2024) 116651.
- [36] D. Song, S. Dai, W. Li, T. Ren, Z. Wei, A.-A. Liu, Stvformer: A spatial-temporal-variable transformer with auxiliary knowledge for sea surface temperature prediction, *Applied Ocean Research* 153 (2024) 104218.
- [37] J. Wang, J. Liu, H. Wang, M. Zhou, G. Ke, L. Zhang, J. Wu, Z. Gao, D. Lu, A comprehensive transformer-based approach for high-accuracy gas adsorption predictions in metal-organic frameworks, *Nature Communications* 15 (1) (2024) 1904.
- [38] P. Pokhrel, E. Ioup, J. Simeonov, M. T. Hoque, M. Abdelguerfi, A transformer-based regression scheme for forecasting significant wave heights in oceans, *IEEE Journal of Oceanic Engineering* 47 (4) (2022) 1010–1023.
- [39] A. Zeng, M. Chen, L. Zhang, Q. Xu, Are transformers effective for time series forecasting?, in: *Proceedings of the AAAI Conference on Artificial Intelligence*, Vol. 37, 2023, pp. 11121–11128.
- [40] A. Gu, T. Dao, Mamba: Linear-time sequence modeling with selective state spaces, *arXiv preprint arXiv:2312.00752* (2023).
- [41] A. Liang, X. Jiang, Y. Sun, C. Lu, Bi-mamba4ts: Bidirectional mamba for time series forecasting, *arXiv preprint arXiv:2404.15772* (2024).
- [42] Q. Li, J. Qin, D. Cui, D. Sun, D. Wang, Cmmamba: channel mixing mamba for time series forecasting, *Journal of Big Data* 11 (1) (2024) 153.
- [43] L. Wu, W. Pei, J. Jiao, Q. Zhang, Umambatsf: A u-shaped multi-scale long-term time series forecasting method using mamba, *arXiv preprint arXiv:2410.11278* (2024).

- [44] Z. Wang, F. Kong, S. Feng, M. Wang, X. Yang, H. Zhao, D. Wang, Y. Zhang, Is mamba effective for time series forecasting?, arXiv preprint arXiv:2403.11144 (2024).
- [45] J. Hu, D. Lan, Z. Zhou, Q. Wen, Y. Liang, Time-ssm: Simplifying and unifying state space models for time series forecasting, arXiv preprint arXiv:2405.16312 (2024).
- [46] Z. Hu, N. A. Daryakenari, Q. Shen, K. Kawaguchi, G. E. Karniadakis, State-space models are accurate and efficient neural operators for dynamical systems, arXiv preprint arXiv:2409.03231 (2024).
- [47] C.-W. Cheng, J. Huang, Y. Zhang, G. Yang, C.-B. Schönlieb, A. I. Aviles-Rivero, Mamba neural operator: Who wins? transformers vs. state-space models for pdes, arXiv preprint arXiv:2410.02113 (2024).
- [48] T. Zhang, X.-Q. Zheng, M.-X. Liu, Multiscale attention-based lstm for ship motion prediction, *Ocean Engineering* 230 (2021) 109066.
- [49] H. Abbasimehr, R. Paki, Improving time series forecasting using lstm and attention models, *Journal of Ambient Intelligence and Humanized Computing* 13 (1) (2022) 673–691.
- [50] S. F. Stefenon, L. O. Seman, L. S. Aquino, L. dos Santos Coelho, Wavelet-seq2seq-lstm with attention for time series forecasting of level of dams in hydroelectric power plants, *Energy* 274 (2023) 127350.
- [51] S. Ma, Y. Kang, P. Bai, Y.-B. Zhao, Fmamba: Mamba based on fast-attention for multivariate time-series forecasting, arXiv preprint arXiv:2407.14814 (2024).
- [52] W. Zhang, J. Huang, R. Wang, C. Wei, W. Huang, Y. Qiao, Integration of mamba and transformer–mat for long-short range time series forecasting with application to weather dynamics, arXiv preprint arXiv:2409.08530 (2024).
- [53] O. Lieber, B. Lenz, H. Bata, G. Cohen, J. Osin, I. Dalmedigos, E. Safahi, S. Meirum, Y. Belinkov, S. Shalev-Shwartz, et al., Jamba: A hybrid transformer-mamba language model, arXiv preprint arXiv:2403.19887 (2024).

- [54] R. Xiong, Y. Yang, D. He, K. Zheng, S. Zheng, C. Xing, H. Zhang, Y. Lan, L. Wang, T. Liu, On layer normalization in the transformer architecture, in: International Conference on Machine Learning, PMLR, 2020, pp. 10524–10533.
- [55] Y. Censor, Pareto optimality in multiobjective problems, *Applied Mathematics and Optimization* 4 (1) (1977) 41–59.
- [56] Y. Lee, S. Liu, J. Darbon, G. E. Karniadakis, Automatic discovery of optimal meta-solvers via multi-objective optimization, arXiv preprint arXiv:2412.00063 (2024).
- [57] I. I. Cplex, V12. 1: User’s manual for cplex, International Business Machines Corporation 46 (53) (2009) 157.
- [58] R. Sergazinov, E. Chun, V. Rogovchenko, N. Fernandes, N. Kasman, I. Gaynanova, Glucobench: Curated list of continuous glucose monitoring datasets with prediction benchmarks, arXiv preprint arXiv:2410.05780 (2024).
- [59] S. Broll, J. Urbanek, D. Buchanan, E. Chun, J. Muschelli, N. M. Punjabi, I. Gaynanova, Interpreting blood glucose data with r package iglu, *PloS One* 16 (4) (2021) e0248560.
- [60] Y. Deng, K. Arao, C. S. Mantzoros, G. E. Karniadakis, Patient-specific deep offline artificial pancreas for blood glucose regulation in type 1 diabetes, *bioRxiv* (2022) 2022–10.
- [61] A. Paszke, S. Gross, F. Massa, A. Lerer, J. Bradbury, G. Chanan, T. Killeen, Z. Lin, N. Gimelshein, L. Antiga, et al., PyTorch: An Imperative Style, High-Performance Deep Learning Library, *Advances in Neural Information Processing Systems* 32 (2019).
- [62] H. Hersbach, B. Bell, P. Berrisford, G. Biavati, A. Horányi, J. Muñoz Sabater, J. Nicolas, C. Peubey, R. Radu, I. Rozum, D. Schepers, A. Simmons, C. Soci, D. Dee, J.-N. Thépaut, Era5 hourly data on single levels from 1940 to present, <https://doi.org/10.24381/cds.adbb2d47>, accessed on DD-MMM-YYYY (2023). doi:10.24381/cds.adbb2d47.
- [63] W. Cummins, W. Iiuhl, A. Uinm, The Impulse Response Function and Ship Motions, *Schiffstechnik* (1962).

- [64] O. Faltinsen, *Sea Loads on Ships and Offshore Structures*, Vol. 1, University Press, 1993.
- [65] J. Pinkster, Mean and low frequency wave drifting forces on floating structures, *Ocean Engineering* 6 (6) (1979) 593–615.
- [66] C. Lee, J. Newman, *Wamit user manual*, version 7.0, wamit, Inc., Chestnut Hill, MA 492 (2013).
- [67] T. Akiba, S. Sano, T. Yanase, T. Ohta, M. Koyama, Optuna: A next-generation hyperparameter optimization framework, in: *Proceedings of the 25th ACM SIGKDD International Conference on Knowledge Discovery and Data Mining*, 2019.